Article

Synthesis and Characterization of a Polydioxanone-Coated Dipeptide-Functionalized Magnetic γ-Fe$_2$O$_3$ Nanoparticles-Modified PES Membrane and Its Biological Applications

Özlem Demirci [1], Serpil Gonca [2], Veysel Tolan [3], Sadin Özdemir [4], Nadir Dizge [5,*] and Ersin Kılınç [6,7,*]

[1] Department of Biology, Science Faculty, Dicle University, 21280 Diyarbakır, Turkey
[2] Department of Pharmaceutical Microbiology, Faculty of Pharmacy, Mersin University, 33343 Mersin, Turkey
[3] Department of Molecular Biology and Genetic, Science Faculty, Dicle University, 21280 Diyarbakır, Turkey
[4] Food Processing Programme, Technical Science Vocational School, Mersin University, 33343 Mersin, Turkey
[5] Department of Environmental Engineering, Mersin University, 33343 Mersin, Turkey
[6] Department of Chemistry and Chemical Processing Technologies, Vocational School of Technical Sciences, Dicle University, 21280 Diyarbakır, Turkey
[7] CanceRNA Biotechnology, Dicle Technocity, 21280 Diyarbakır, Turkey
[*] Correspondence: ndizge@mersin.edu.tr (N.D.); kilincersin@gmail.com (E.K.)

Abstract: This work is focused on the synthesis of leucyl-glycine-functionalized γ-Fe$_2$O$_3$ magnetic nanoparticles coated by polydioxanone (γ-Fe$_2$O$_3$-CA-Leu-Gly-PDX) as a polyethersulphone (PES) membrane for biotechnological applications. The physicochemical characteristics were investigated by FT-IR, SEM, XRD, a vibrating sample magnetometer (VSM), and ICP-OES. The present investigation also centered on the several biological activities of γ-Fe$_2$O$_3$-CA-Leu-Gly-PDX. The 2,2-diphenyl-1-picrylhydrazyl (DPPH) radical scavenging and metal chelating activity was studied for evaluation of its antioxidant activity potential. It exhibited 100% DPPH radical scavenging and 93.33% metal chelating activity. With applicability to antimicrobial photodynamic therapy, DNA cleavage and antimicrobial activity, the cell viability of γ-Fe$_2$O$_3$-CA-Leu-Gly-PDX was investigated in detail. The γ-Fe$_2$O$_3$-CA-Leu-Gly-PDX demonstrated the significant biofilm inhibition activity as being 81.54% and 86.34% for *P. aeruginosa* and *S. aureus*, respectively. Moreover, a novel polyethersulphone nanocomposite membrane incorporated with γ-Fe$_2$O$_3$-CA-Leu-Gly-PDX was prepared. The performance of the γ-Fe$_2$O$_3$-CA-Leu-Gly-PDX-blended polyethersulphone (PES) membrane was investigated by measuring the antifouling and *E. coli* rejection. The nanocomposite membranes demonstrated remarkable antifouling properties in contrast with the pristine PES when BSA (bovine serum albumin) and *E. coli* were filtrated. A complete rejection was obtained by the composite membrane. After an application of the membrane study, the modified polyethersulphone (PES) membrane blended with γ-Fe$_2$O$_3$-CA-Leu-Gly-PDX removed 100% of the *E. coli*.

Keywords: magnetic nanomaterials; nanocomposite PES membrane; protein separation; *E. coli*; biotechnology

1. Introduction

Environmental contaminations due to anthropogenic activities threaten water resources as well as causing air, soil, food, etc., contamination. Pollutants can be originated from organics such as persistent organic pollutants, dyes, etc., as well as from inorganics such as toxic metal ions and their complexes and living systems such as bacteria, viruses, etc. [1]. Various methods have been recommended for their usability to reduce environmental pollution such as chemical, physical and biotechnological methods; however, environmentally friendly technologies are urgently required to reduce pollution and provide a livable environment [2–4].

Recently, membranes originating from polymers have been used for filtration in a variety of targets including for suspended and dissolved particles [5,6]. With an applicability to various water/wastewater treatment processes, their high separation efficiency and low cost could be evaluated as having advantages over other methods [7–9]. Although there are many polymeric materials for membrane filtration, polyethersulphone (PES), with its hydrophobic surface, is the most widely used due to its extraordinary resistance to strong chemicals, commercial availability, easy processing and thermal features [10,11].

In recent years, surface modifications through covalent chemistry have attained a special focus that importantly also contributes the polymeric membranes' characteristics [12–15]. From this point of view, polyethersulphone (PES) with its advantages, for example, of its resistance to heat-aging and stability under a high temperature could be accepted as the starting polymeric material for further functionalization [16]. On the other hand, there are some disadvantages such as its permeability to water flux and antifouling that should be solved. To overcome this problem many nanomaterials such as Cu_2ZnSnS_4 nanoparticles [17], Zirconium phosphate (PES/α-ZrP) flat-sheet [18], nitrogen-doped porous graphene [19], hydrogen peroxide-treated g-C_3N_4 [20], nanocrystalline cellulose-incorporated biopolymer [21], and NaY zeolite [22] have been strongly investigated to improve the performance of PES membranes. The results have showed that the surface modifications of PES membrane critically increase their biotechnological applications.

Peptides are known as versatile compounds that are found naturally. Some peptides, including Leu-Gly, can form a peptide nanotube as a self-assembly [23]. Leu-Gly, was selected as the dipeptide for the first layer coating of γ-Fe_2O_3 [24]. Cationic Leu-Gly-rich peptides are known as being hemolytic and have strong activity versus microorganisms [25]. It was also reported that Leu-Gly is a main member of the collagen-model triplehelical peptides [26].

In this research paper, a γ-Fe_2O_3 magnetic nanoparticle was selected as the core material for further functionalization with citric acid, Leucine-Glycine dipeptide and polydioxanone (γ-Fe_2O_3-CA-Leu-Gly-PDX). It was functionally designed and synthesized. It should be noted that the recommended material could be guided by a magnetic field due to its superparamagnetic nature. The physicochemical details were investigated by infrared spectroscopy, scanning electron microscopy, and X-ray diffraction spectroscopy. The main idea was to coat the superparamagnetic γ-Fe_2O_3 nanoparticles using a Leu-Gly dipeptide that our metabolism recognizes. The outermost layer of the functionalized nanoparticle prepared was covered with polydioxanone, while surface techniques were employed for the characterization. The antifouling properties and separation ability of the developed γ-Fe_2O_3-CA-Leu-Gly-PDX nanoparticles-blended PES membrane were investigated by using a model solution of *E. coli*.

2. Results and Discussions

2.1. Surface Characterization

FT-IR was used to investigate the variation of the chemical structure of the surface (Figure 1A). The broad band at approximately 3400–3500 cm^{-1} showed the presence of surface hydroxyls of γ-Fe_2O_3, as shown in Figure 1A. The peaks at 632 and 585 cm^{-1} were characteristic peaks for Fe-O vibrations of γ-Fe_2O_3. The peak at nearly 1600 cm^{-1} was attributed to a C=O vibration from the carboxyl group of citric acid as shown in Figure 1A [27]. There were no significant differences observed after coating with the Leu-Gly (Figure 1A(a,b)). This could be from a lack of sensitivity of the FT-IR due to a low amount of Leu-Gly. From Figure 1A(a,c,) the carbonyl of PDX (C=O stretching vibration) was observed at approximately 1735 cm^{-1} as well as CH$_2$ bending at 1386 cm^{-1}, and CO stretching at 1233 and 1109 cm^{-1} [28].
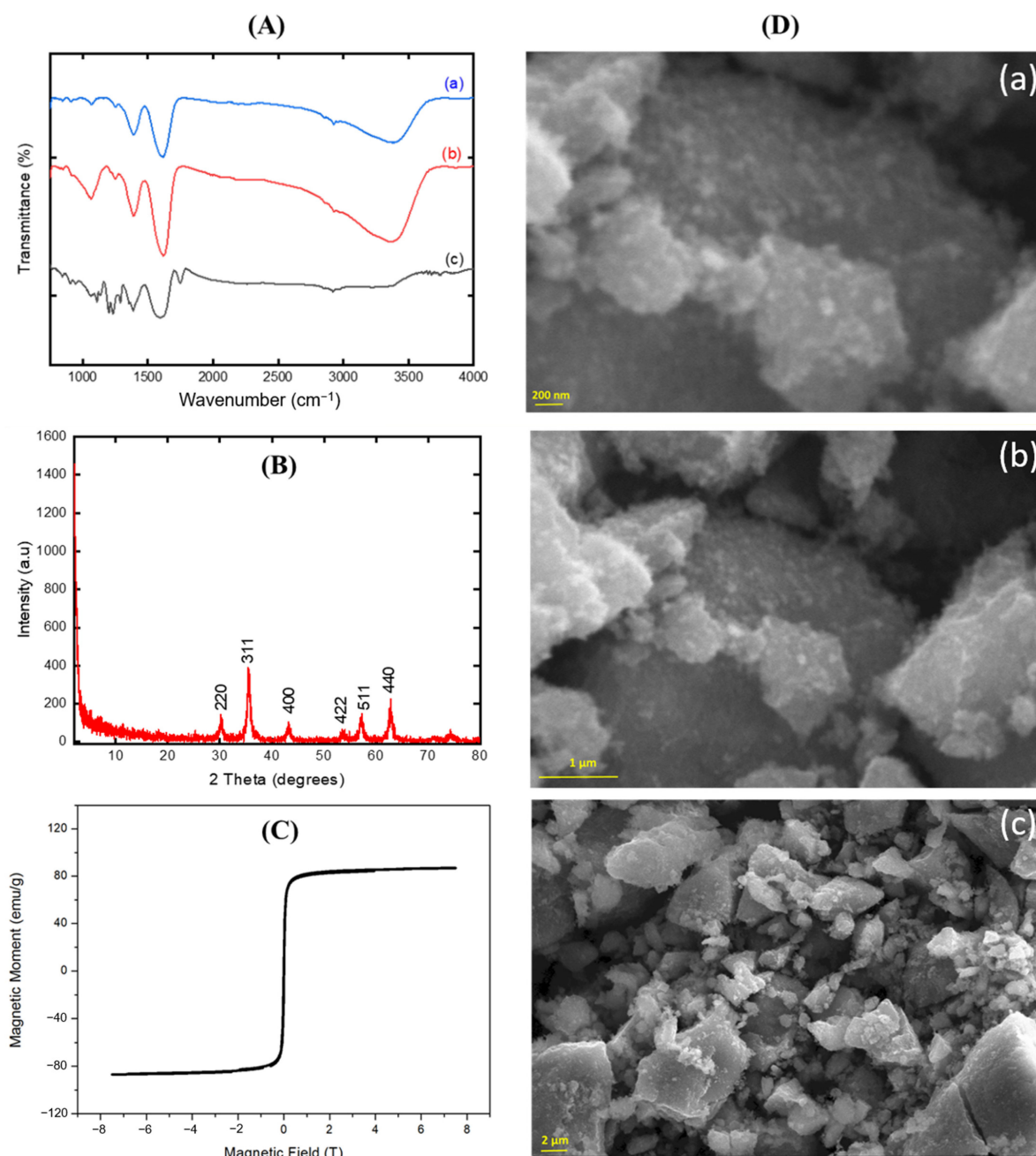
Figure 1. (**A**) FT-IR spectral comparison of (a) γ-Fe$_2$O$_3$-CA, (b) γ-Fe$_2$O$_3$-CA-Leu-Gly-CDP, and (c) γ-Fe$_2$O$_3$-CA-Leu-Gly-PDX, (**B**) XRD pattern of γ-Fe$_2$O$_3$-CA-Leu-Gly-PDX, (**C**) VSM magnetization curve of γ-Fe$_2$O$_3$-CA-Leu-Gly-PDX, and (**D**) SEM image of γ-Fe$_2$O$_3$-CA-Leu-Gly-PDX at different resolutions of (a) 200 nm, (b) 1 μm, and (c) 2 μm.

The structure of the magnetic nanoparticles was confirmed by considering the results from the XRD (Figure 1B). A series of characteristic peaks at 2θ = 30.5°, 35.8°, 43.8°, 54.2°, 57.7°, and 63.2°, which corresponded to (220), (311), (400), (422), (511), and (440) Bragg reflection, respectively, in Figure 1A, agreed with the standard maghemite (γ-Fe$_2$O$_3$) XRD patterns (Maghemite-Q, Card No. 25-1402). By comparing the XRD spectra with the literature, there was a clear verification of the crystal structure of the synthesized core of the magnetic nanoparticles as being γ-Fe$_2$O$_3$ [29–32].

The magnetic properties of the γ-Fe$_2$O$_3$-CA-Leu-Gly-PDX was investigated by VSM. The magnetization curve is presented in Figure 1C. A 85.6 emu/g saturation for the magnetization was measured and this confirmed the superparamagnetic characteristics. It

should be highlighted that all of the components of the γ-Fe$_2$O$_3$-CA-Leu-Gly-PDX had no toxicity present and could be applied to the body directly for diagnostics and therapy via a controlled drug delivery. The Fe concentrations in the pristine γ-Fe$_2$O$_3$-CA-Leu-Gly-PDX were measured by ICP-OES. This was determined as 11,108 mg/kg of Fe.

SEM was employed to investigate the microstructure and morphology of the γ-Fe$_2$O$_3$-CA-Leu-Gly-PDX (Figure 1D), which showed a uniform size distribution.

2.2. Antimicrobial Properties of γ-Fe$_2$O$_3$-CA-Leu-Gly-PDX Nanoparticles

2.2.1. DPPH Radical Scavenging Activity of γ-Fe$_2$O$_3$-CA-Leu-Gly-PDX

The antioxidant activities were investigated by using the DPPH method. The most important reasons for using this method are its high accuracy, and it is an inexpensive, simple and fast method. The results of the leucyl-glycine (Leu-Gly) functionalized-γ-Fe$_2$O$_3$ magnetic nanoparticles following a biocompatible coating via polydioxanone [γ-Fe$_2$O$_3$-CA-Leu-Gly-PDX] DPPH scavenging activity is shown in Figure 2. The radical scavenging activity of the γ-Fe$_2$O$_3$-CA-Leu-Gly-PDX was found as 68.46, 81.02, 90.76, and 96.66% at concentrations of 12.5, 25, 50, and 100 mg/L, respectively. The highest activity at 100% was obtained for the 200 mg/L concentration. The γ-Fe$_2$O$_3$-CA-Leu-Gly-PDX showed significant radical scavenging activity when compared with the standard antioxidants. It was pointed out that a new type of iron oxide nanoparticles were green synthesized and characterized [33]. The antioxidant activity of the iron oxide nanoparticles by the DPPH scavenging process were investigated and the radical scavenging activity was found approximately at 20% at a concentration of 100 mg/L [34]. Additionally, avidin-coated and uncoated Fe@Au nanoparticles were investigated using the DPPH process for their antioxidant activities [35]. The avidin-coated NPs showed a higher DPPH scavenging activity than avidin uncoated Fe@Au nanoparticles. It was also found that the radical scavenging antioxidant activity was increased when the concentration increased. Shah et al. prepared three types of gallic acid-modified iron oxide nanoparticles (IONPs@GA) [36]. They investigated the DPPH scavenging activity of all the IONPs@GA samples and unfunctionalized IONP. The radical scavenging activity was found to be between 59–78%, and 50% for the unfunctionalized IONP, respectively, at 10^{-4} M. Our results indicated that γ-Fe$_2$O$_3$-CA-Leu-Gly-PDX can be used as an antioxidant agent for reducing the risk of cancer after further studies.
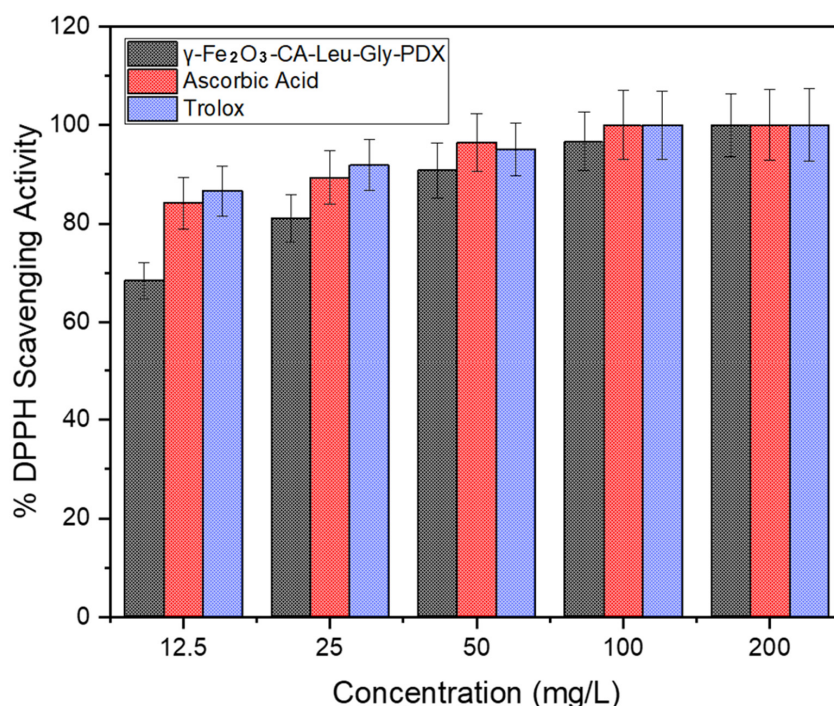

Figure 2. DPPH scavenging activity of γ-Fe$_2$O$_3$-CA-Leu-Gly-PDX.

2.2.2. Ferrous Ion Chelating Activity of γ-Fe$_2$O$_3$-CA-Leu-Gly-PDX

Most of the reactive oxygen species (ROS) are produced as by-products throughout the electron transport system and other physiological and biochemical reactions. For the transition metal ion, however, it is well known that Fe^{2+} has the ability to sustain free radical generation through redox reactions. Since excessive iron and other free metal ions play a role in the induction and generation of free radicals in living organisms, we investigated the γ-Fe$_2$O$_3$-CA-Leu-Gly-PDX in a ferrous chelating activity test. The γ-Fe$_2$O$_3$-CA-Leu-Gly-PDX demonstrated a concentration-dependent metal chelating activity (Figure 3). When the concentration of the γ-Fe$_2$O$_3$-CA-Leu-Gly-PDX increased from 12.5 mg/L to 25 mg/L, the metal chelating activity increased from 37.03% to 52.41%, respectively. The metal chelating activity was also 71.18 and 83.88% at concentrations of 50 and 100 mg/L, respectively. The maximum metal chelating activity of the γ-Fe$_2$O$_3$-CA-Leu-Gly-PDX was found to be 93.33% at 200 mg/L. Madhu et al. reported that they synthesized and characterized a green iron oxide nanoparticle by using a *Solanum tuberosum* extract [37]. They also investigated the metal chelating activity of iron oxide NPs and found that new synthesized iron oxide NPs exhibited good metal activity. According to our findings, γ-Fe$_2$O$_3$-CA-Leu-Gly-PDX can be used as a metal chelating agent.
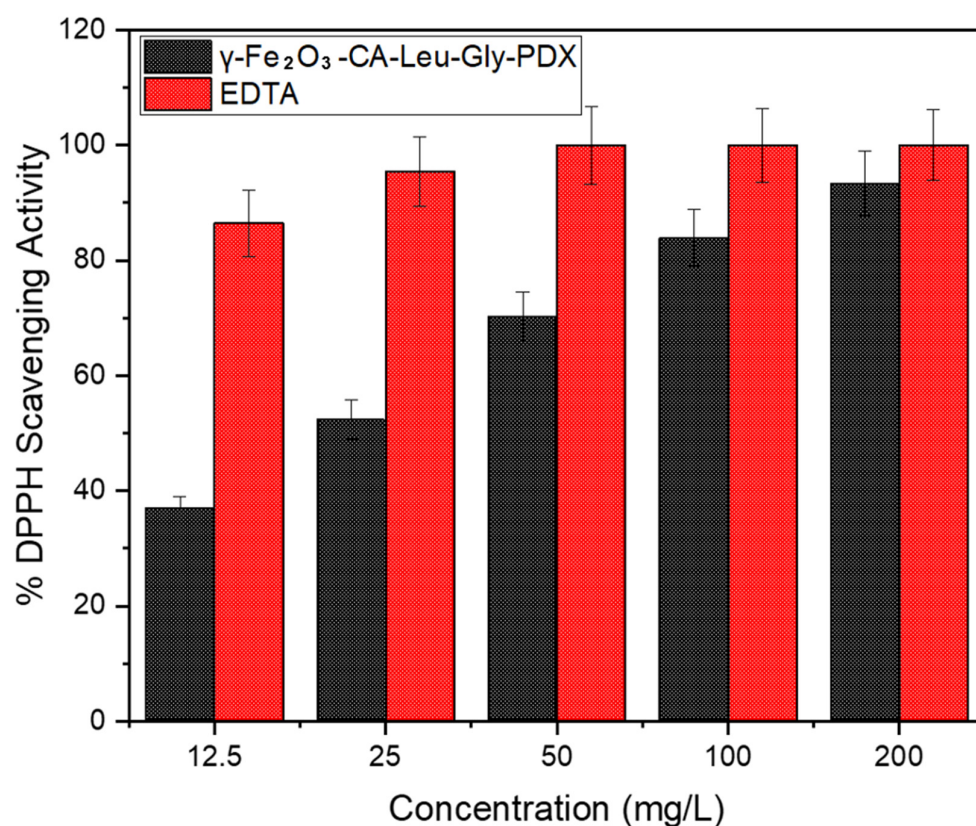
Figure 3. Metal chelating activity of γ-Fe$_2$O$_3$-CA-Leu-Gly-PDX.

2.2.3. Antimicrobial Activity

The antimicrobial activity of the γ-Fe$_2$O$_3$-CA-Leu-Gly-PDX was investigated by using a micro-dilution process (Table 1). The MIC value was determined as 256 mg/L for *P. aeruginosa*, *L. pneumophila* and *C. tropicalis*, 128 mg/L for *E. hirae*, *S. aureus*, and *C. parapisilosis* and 64 mg/L *E. fecalis*. According to these results, Gram-positive bacteria was more sensitive than Gram-negative bacteria and the most sensitive microorganism was *E. fecalis*. There are several investigations on the antimicrobial activity of IONPs in the literature. Rufus et al. green synthesized α-Fe$_2$O$_3$ NPs from the extract of *Psidium guajava* leaves [38]. They indicated that α-Fe$_2$O$_3$ NPs exhibited antimicrobial activity against both Gram-positive and Gram-negative bacteria. Naseem and Farrukh reported that they studied the antibacterial

activity of iron NPs and revealed that synthesized-iron NPs showed a moderate antimicrobial effect against *Escherichia coli*, *Proteus mirabilis*, *Salmonella enterica*, and *Staphylococcus aureus* [39]. Rafi et al. synthesized and characterized iron nanoparticles on polysaccharides templates (agarose, dextran and gelatin) and they also investigated the antimicrobial activity of iron NPs on polysaccharides templates [40]. It was also reported that an antimicrobial study demonstrated an inhibition against *Aeromonas hydrophila* and *Escherichia coli*. It was also found that silver and iron oxide nanoparticles with a biosurfactant coating were demonstrated to be more effective against Gram-positive bacteria than Gram-negative bacteria for antimicrobial activity [41]. This difference may be owing to the thickness and differences in cell wall compositions. Metal ions released from polydioxanone-coated iron NPs may have caused the generation of reactive oxygen species, resulting in an antimicrobial effect [42]. A similar phenomenon was reported by Turakhia et al. who revealed that the mechanism by which the iron oxide NPs demonstrated antimicrobial activity may have been owing to the oxidative stress process created by reactive oxygen species (ROS), which can disrupt cellular macromolecules [43]. Shi et al. reported that they prepared chitosan-coated iron oxide nanoparticles, and they also studied the antimicrobial effect of chitosan-coated iron oxide nanoparticles. Their results revealed that the chitosan-coated iron oxide nanoparticles displayed antibacterial activity [44]. Inbaraj et al. investigated poly(gamma-glutamic acid)-coated magnetite nanoparticles that they synthesized and characterized and tested the poly(gamma-glutamic acid)-coated magnetite nanoparticles for antimicrobial activity. Their results showed that it was demonstrated to have an antimicrobial effect [45]. In addition to these MNPs, several derivatives, such as those that were Co-doped, Ag-coated, Au-coated, and cationic polymer-modified, were also investigated for their antimicrobial and antibiofilm formation. They were shown to penetrate into microbial cells and biofilm aggregate, which can inhibit bacteria and antibiotic-resistant bacteria [46–50].

Table 1. The minimum inhibition concentration (MIC) of test microorganisms.

Microorganisms	γ-Fe$_2$O$_3$-CA-Leu-Gly-PDX *
E. coli	512
P. aeruginosa	256
L. pneumophila subsp. *pneumophila*	256
E. hirae	128
E. fecalis	64
S. aureus	128
C. parapisilosis	128
C. tropicalis	256

* mg/L.

2.2.4. DNA Cleavage Ability

DNA fragmentation is an essential property of apoptosis, a form of programmed cellular death. The DNA is reduced to smaller pieces of oligonucleosomal size and visualized as a ladder pattern in an agarose gel electrophoresis; therefore, agents that cause DNA fragmentation are of great importance in cancer and antimicrobial studies. Agarose gel electrophoresis is the easiest, fastest and most effective chromatographic method used in the determination of DNA molecules. The DNA cleavage activity of the γ-Fe$_2$O$_3$-CA-Leu-Gly-PDX was performed at different concentrations by using an agarose gel electrophoresis process. The result of the DNA cleavage activity assay is represented in Figure 4. As shown in Figure 4, the new synthesized γ-Fe$_2$O$_3$-CA-Leu-Gly-PDX displayed single strand DNA cleavage activity at 50, 100 and 200 mg/L concentrations. Rehana et al. synthesized and characterized iron oxide nano particles and showed that L-arginine-coated nanoparticles exhibited DNA cleavage activity which was observed as a DNA fragmentation by agarose gel electrophoresis [51]. Palchoudhury et al. reported that they synthesized and charac-

terized Pt-attached iron oxide nanoparticles [52]. The DNA interaction and cleavage of small Pt NP-attached iron oxide NPs were also investigated and it was determined that the Pt-attached iron oxide NPs demonstrated DNA cleavage activity. Additionally, metallic nanoparticles can also increase oxidative stress via a ROS formation followed by more DNA oxidation [53,54]. According to the results, the antimicrobial activity mechanism of γ-Fe$_2$O$_3$-CA-Leu-Gly-PDX can be reasoned by its DNA cleavage activity.
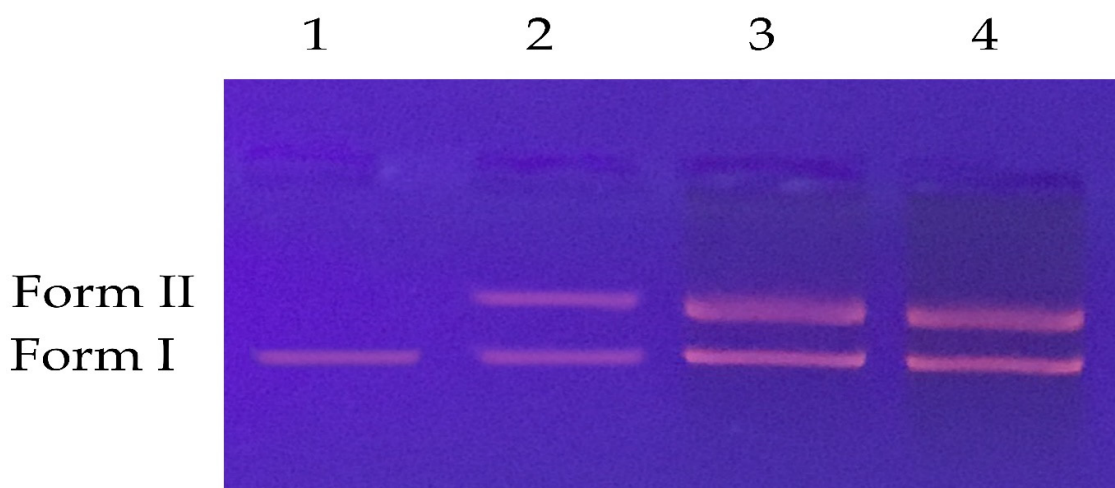
Figure 4. DNA cleavage activity of synthesized γ-Fe$_2$O$_3$-CA-Leu-Gly-PDX. Lane 1, pBR 322 DNA; Lane 2, pBR 322 DNA + 50 mg/L of γ-Fe$_2$O$_3$-CA-Leu-Gly-PDX; Lane 3, pBR 322 DNA + 100 mg/L of γ-Fe$_2$O$_3$-CA-Leu-Gly-PDX; Lane 4, pBR 322 DNA + 200 mg/L of γ-Fe$_2$O$_3$-CA-Leu-Gly-PDX.

2.2.5. Microbial Cell Viability

Magnetite nanoparticles (Fe$_3$O$_4$) have superb properties that make them promising agents for antimicrobial usages. The reinforcing impacts of magnetic NPs bind to the microbial cell walls, causing the cell membrane to deteriorate.The microbial cell viability of γ-Fe$_2$O$_3$-CA-Leu-Gly-PDX was investigated against *E. coli* and the results of the microbial cell viability test are demonstrated in Figure 5. The new synthesized γ-Fe$_2$O$_3$-CA-Leu-Gly-PDX showed significant antibacterial activity. After being treated with various concentrations of γ-Fe$_2$O$_3$-CA-Leu-Gly-PDX, the *E. coli* growth was inhibited as 86.17, 98.25, and 100% at 125, 250 and 500 mg/L, respectively. Naha et al. reported that microbial cell viability was significantly reduced by using 1.5, 5, and 10 kDa dextran-coated iron oxide nanoparticles and it was also indicated that 25 and 40 kDa-coated iron oxide nanoparticles exhibited lower microbial cell viability than 1.5, 5 and 10 kDa dextran-coated iron oxide nanoparticles [55]. Shi et al. reported that chitosan-coated iron oxide nanoparticles showed a biofilm inhibition by *S. aureus* and it was also determined that the amount of microbial cell viability was significantly decreased [44]. Metal oxide nanoparticles are of particular attention as antimicrobial agents as they can be prepared with multiple edges, a high surface-to-volume ratio, have unusual crystal morphologies with multiple corners and other potentially reactive areas. Due to the high surface-to-volume ratio of nanoparticles, they can interact with microbial membranes and damage their membrane structures directly or indirectly and cause the microorganisms to be inactivated [56]. In addition to these, iron NPs can cause the disruption of membrane transport processes, the deterioration of protein folding and conformation, and protein aggregation. These effects may also cause antimicrobial activity.
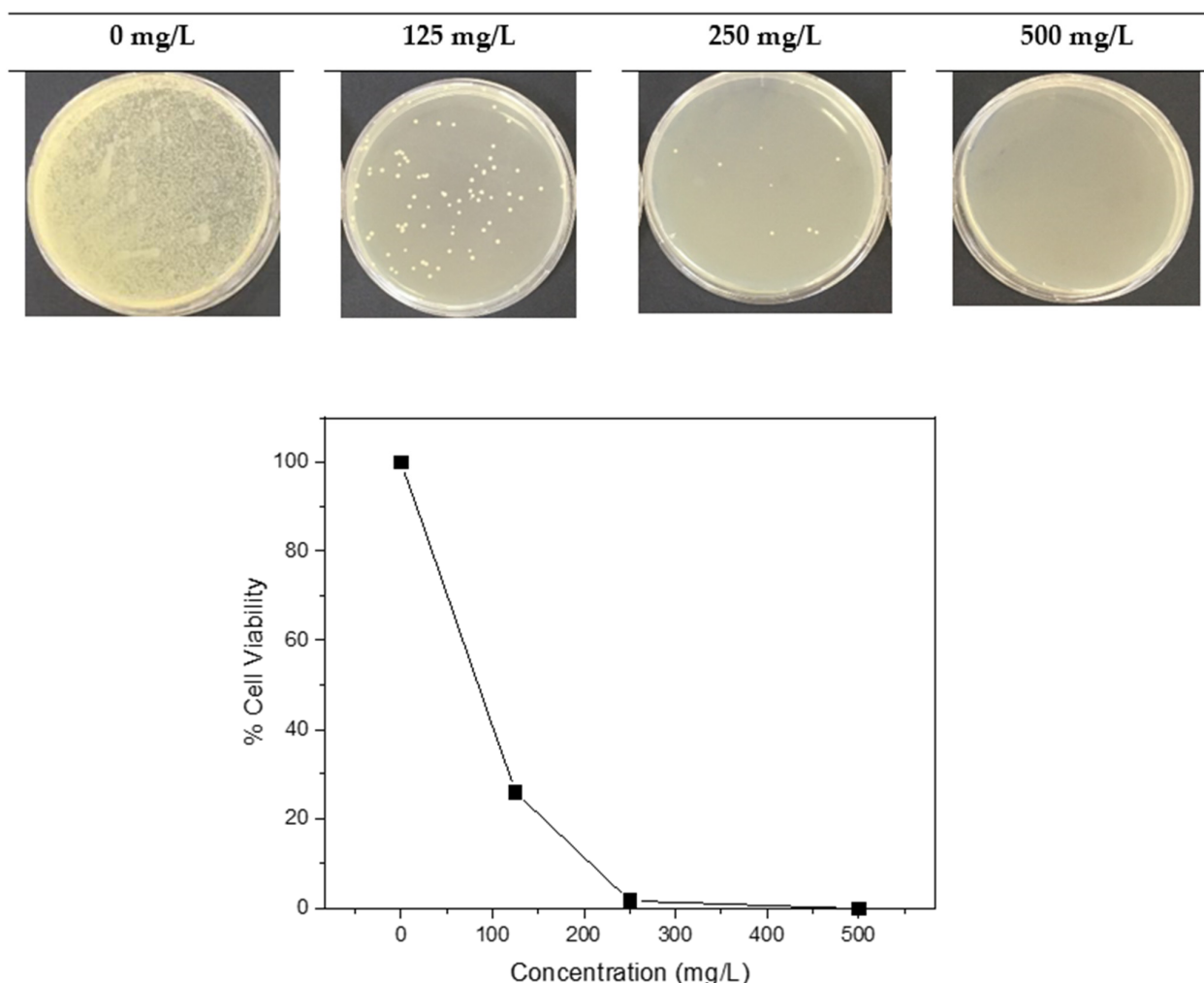
Figure 5. Microbial cell viability.

2.2.6. Antimicrobial Photodynamic Therapy by γ-Fe$_2$O$_3$-CA-Leu-Gly-PDX

Antimicrobial photodynamic therapy (aPDT) uses a suitable excitation light source with photosensitizers (PSs) and oxygen. Reactive oxygen species (ROS), especially singlet oxygens, are released after a light treatment and non-specific attacks occur from cytotoxic ROS against microorganisms. This strong oxidation and the high reactive agents cause the rapid lipid oxidation of bacteria. As a result, the membrane structure breaks down and, eventually, microbial death occurs [57]. The antimicrobial photodynamic therapy (aPDT) by γ-Fe$_2$O$_3$-CA-Leu-Gly-PDX was investigated by using LED irradiation against *E. coli* for 120 min. The results of the aPDT are shown in Figure 6. Iron oxide nanoparticles can be used like photosynthesis. As seen in Figure 6, the γ-Fe$_2$O$_3$-CA-Leu-Gly-PDX inhibited the microbial growth by 98% and 99.99% at 25 and 50 mg/L, respectively, in the dark, while a 100% cell inhibition was observed in the γ-Fe$_2$O$_3$-CA-Leu-Gly-PDX 25 and 50 mg/L with the LED irradiation. Ma et al. pointed out that Fe$_3$O$_4$-TNS nanosheets demonstrated higher photocatalytic antimicrobial activity against Gram-positive *S. aureus* and Gram-negative *E. coli* than pure TNS and Fe$_3$O$_4$ [58]. It was also reported that the antimicrobial activity was decreased by 87.2% and 93.7% against the *E. coli* and *S. aureus* after 2 h of solar light irradiation at a concentration of 100 μg/mL Fe$_3$O$_4$-TNS, respectively. Pan et al. synthesized and characterized reduced graphene oxide (rGO)-iron oxide nanoparticles (rGO-IONP) and they investigated the antimicrobial photodynamic therapy of rGO-IONP+H$_2$O$_2$ treated with near infrared (NIR) laser irradiation. They observed significant antimicrobial activity when compared with a control group [59].
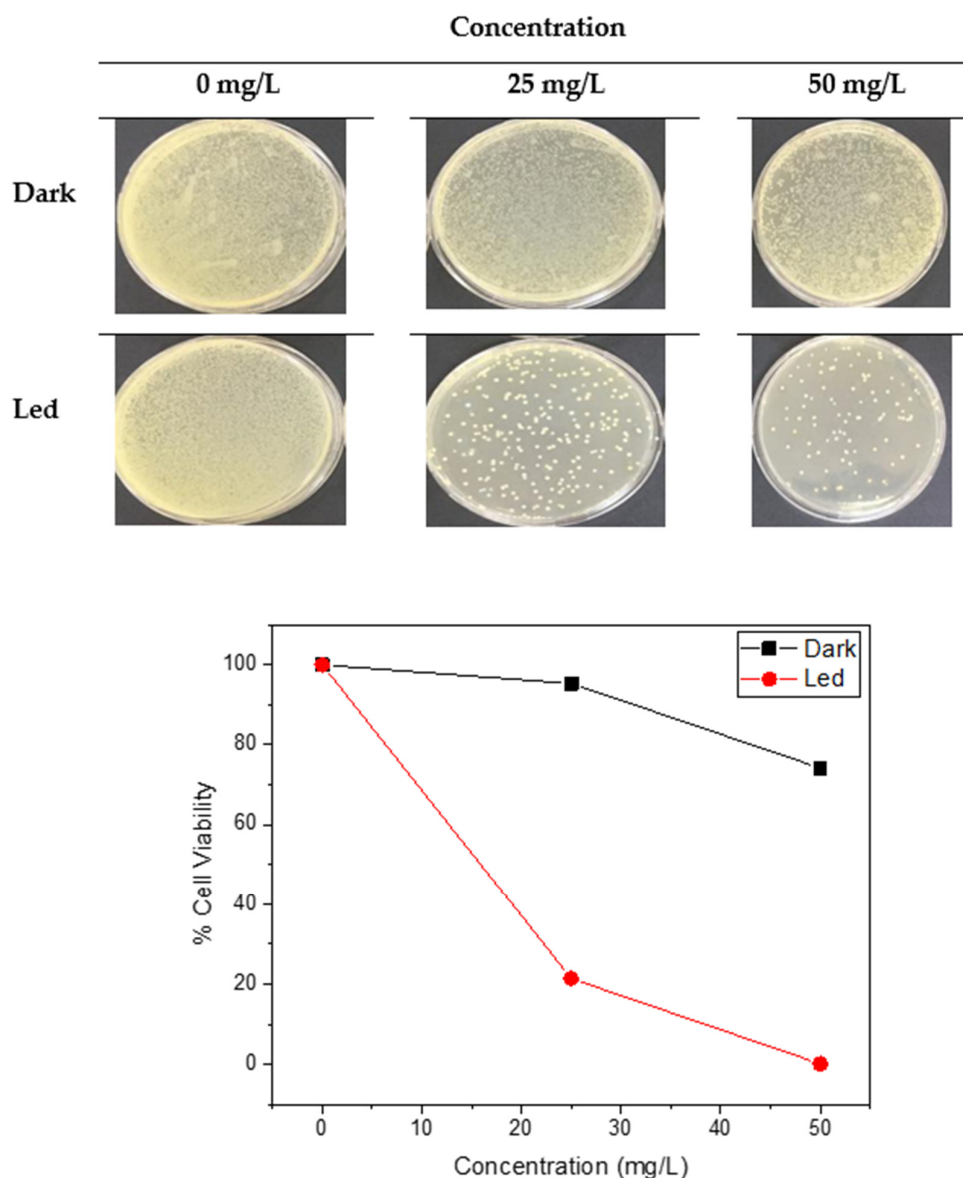
Figure 6. Antimicrobial photodynamic therapy of γ-Fe$_2$O$_3$-CA-Leu-Gly-PDX.

2.2.7. Biofilm Inhibition Activity

Biofilm is a polymeric structure that allows microorganisms to attach to each other or to a surface. This polymeric structure acts as a shield against microorganisms to immune cells and antibiotics. As a result, microorganisms that are highly resistant to antibiotics-application emerge. In addition, they can adhere strongly to medical implant surfaces, causing the contamination of various microbial infectious diseases. For these reasons, interest in agents that prevent biofilm formation is increasing day by day [44]. Here, we investigated the influence of γ-Fe$_2$O$_3$-CA-Leu-Gly-PDX on the biofilm formation of *S. aureus* and *P. aeruginosa* at different concentrations after 72 h of incubation. The results of the biofilm inhibition are depicted in Figure 7. A significant inhibition in the biofilm formation was observed in the presence of the γ-Fe$_2$O$_3$-CA-Leu-Gly-PDX for both test microorganisms. It was also determined that the biofilm inhibition activity of γ-Fe$_2$O$_3$-CA-Leu-Gly-PDX was concentration-dependent. When the concentration increased from 125 mg/L to 250 mg/L, the biofilm inhibition was increased from 53.28% to 69.71% for *S. aureus* and from 51.96% to 65.37% for *P. aeruginosa*. The highest biofilm inhibition was found to be 86.34% and 81.54% for *S. aureus* and *P. aeruginosa* at concentrations of 500 mg/L, respectively. Erci and Cakir-Koc reported on the biofilm inhibition activity of synthesized FeONPs, studied using *S. aureus* as a test microorganism after a 24 h

incubation [34]. According to their results, the highest biofilm inhibition activity was shown at 100 mg/L, at nearly 45%. Thukkaram et al. examined the influence of iron oxide NPs on the formation of biofilm on various bio-material surfaces and pluronic-coated surfaces and it was reported that an effective biofilm inhibition was obtained at a high concentration of iron oxide NPs against *S. aureus*, *E. coli* and *P. aeruginosa* [60]. Sathyanarayanan et al. investigated the impact of gold and iron oxide NPs on *S. aureus* and *P. aeruginosa* biofilms [56] and it was found that the biofilm production was decreased with high concentrations of gold and iron-oxide NPs when compared with a control. Naha et al. investigated the biofilm inhibition using dextran-coated iron oxide nanoparticles and they found that a maximal anti-biofilm activity was obtained with 10 kDa of dextran-coated iron oxide NPs. They also demonstrated that an antibiofilm inhibition occurred via the mechanisms of an EPS-matrix breakdown [55]. It was found that tobramycin-conjugated and alginate-coated iron oxide NPs were demonstrated to inhibit the production of a biofilm by *P. aeruginosa* [61]. Khalid et al. reported on an easy process for the synthesis of rhamnolipid (RL)-coated silver (Ag) and iron oxide (Fe_3O_4) NPs and they also investigated the biofilm inhibition against biofilms produced by *S. aureus* and *P. aeruginosa* [41]. The silver (Ag) and iron oxide (Fe_3O_4) NPs exhibited significant biofilm inhibition activity not only during the biofilm generation but also on preformed biofilms. These ions disrupted the effective electrostatic interaction between bacterial cells in the biofilm, and as a result, these ions penetrated the cell and caused a biofilm inhibition by reducing or blocking the adhesion of the cells to each other [41].
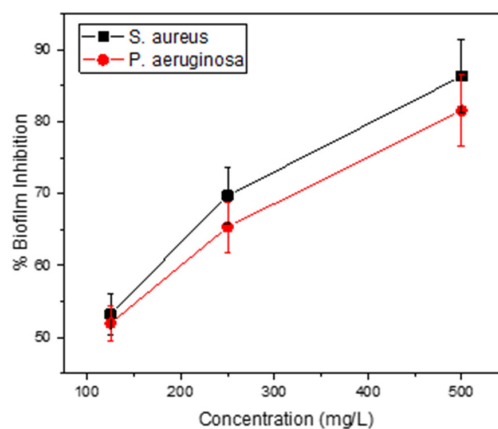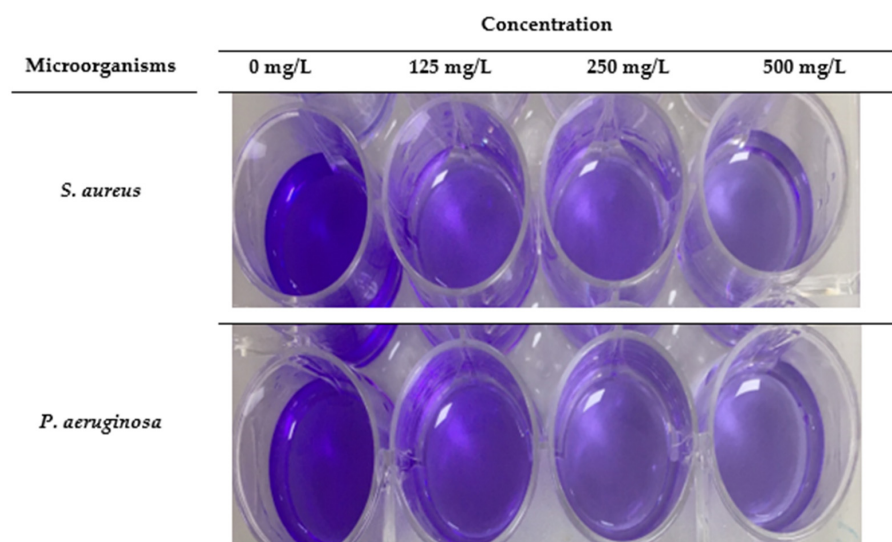
**Figure 7.** Biofilm inhibition of γ-Fe_2O_3-CA-Leu-Gly-PDX.

2.3. Pristine and NPs-Blended Membrane Performance

The mean pore radius and porosity of the pristine and NPs-blended membranes are presented in Table 2. The pore size of the prepared membranes was approximately in the range of UF membranes. The pore radius and porosity of the NPs-blended membrane were higher than the pristine membrane. In addition, the amount of iron released during the filtration process was determined by an AAS analysis, and it was determined that the nanoparticle diffusion from the membrane was negligible 2 h after the experiment.

Table 2. Effect of NPs amount on the mean pore size and porosity properties.

Membrane Sample	Mean Pore Radius (nm)	Porosity (%)	Released Iron in Permeate (µg/L)
Pristine membrane	22.2 $\pm$ 0.5	58.13 $\pm$ 2.85	-
NPs-blended membrane	20.9 $\pm$ 0.4	61.12 $\pm$ 3.22	88 $\pm$ 9

The performance of the pristine and γ-Fe$_2$O$_3$-CA-Leu-Gly-PDX-blended membranes were investigated in a dead-end filtration system for bovine serum albumin (BSA) and *E. coli* fluxes and rejection. The obtained results are shown in Figure 8. As can be seen from Figure 8A, the pristine and NPs-blended composite membranes showed a similar water flux. The water fluxes were calculated as 49.9 $\pm$ 3.2 and 49.3 $\pm$ 2.8 L/m^2/h for the pristine and NPs-blended membranes, respectively. This means that blended NPs do not block the membrane pores; however, a decrease in the flux was observed for the pristine membrane when the BSA was filtrated for 90 min. The BSA fluxes were calculated as 10.7 $\pm$ 2.2 and 18.1 $\pm$ 3.3 L/m^2/h for the pristine and NPs-blended membranes, respectively. After physical cleaning of the membrane surface, the water fluxes were calculated as 32.6 $\pm$ 3.6 and 47.1 $\pm$ 3.8 L/m^2/h for the pristine and NPs-blended membranes, respectively. The results depict that the γ-Fe$_2$O$_3$-CA-Leu-Gly-PDX protected the modified membrane surface against protein fouling.
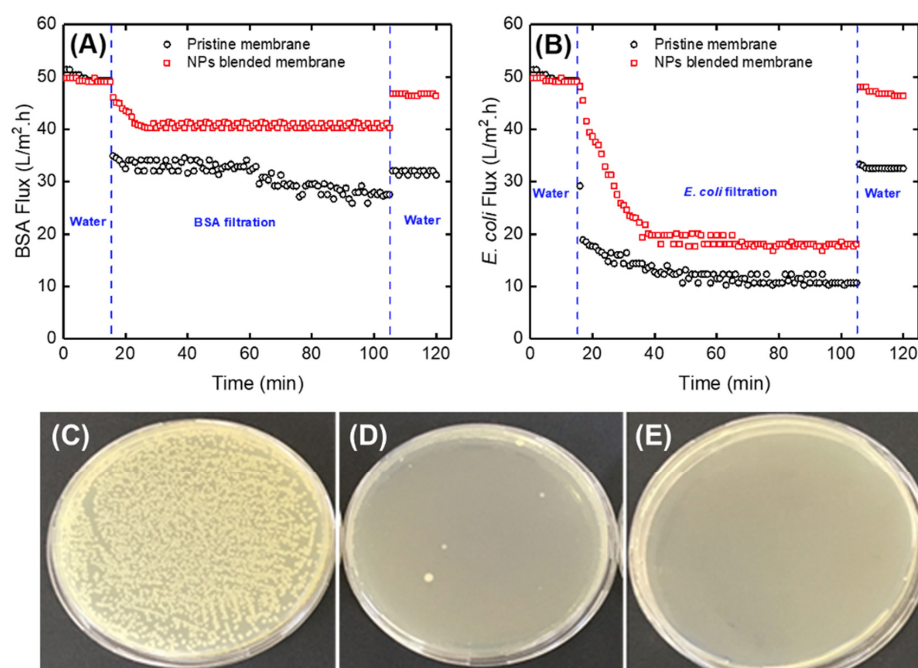
Figure 8. Application of polyethersulphone (PES) membrane blended with γ-Fe$_2$O$_3$-CA-Leu-Gly-PDX for (**A**) BSA flux versus time, (**B**) *E. coli* flux versus time, (**C**) inlet *E. coli* culture (control), (**D**) permeate of PES membrane and (**E**) permeate of modified PES membrane.

The pristine and modified membranes were also tested for *E. coli* filtration (Figure 8B). The fluxes were 27.5 ± 2.5 and 40.3 ± 3.5 L/m^2/h for the pristine and NPs-blended membranes, respectively. After physical cleaning of the membrane surface, the water fluxes were calculated as 31.8 ± 2.7 and 46.7 ± 3.4 L/m^2/h for the pristine and NPs-blended membranes, respectively. The *E. coli* removal results (Figure 8C–E) showed that the pristine and modified membranes removed 99.9% and 100%, respectively.

Table 3 shows the performance comparison of the γ-Fe$_2$O$_3$-CA-Leu-Gly-PDX-blended PES membrane with the other reported modified-PES membranes. From the table, the competitive performance of the PES/γ-Fe$_2$O$_3$-CA-Leu-Gly-PDX composite membrane in terms of an improved BSA and *E. coli* rejection is evident.

Table 3. Performance comparison of PES membranes blended with different NPs.

Material	Model Solution	NPs Amount	Main Results for Modified Membrane	Reference
γ-Fe$_2$O$_3$-CA-Leu-Gly-PDX	BSA *E. coli*	1.0 wt%	• Pure water permeability: 49.3 L/m^2 h bar • BSA removal: 100% • *E. coli* removal: 100% • Porosity: 61.12% • Mean pore radius: 20.9 nm	This study
Fe$_3$O$_4$ decorated halloysite nanoclay (Fe-HNC)	Humic acid (HA)	0.1 wt%	• Pure water permeability: 294.4 L/m^2 h bar • HA removal: 90.1% • High fouling recovery: 70.4 % • Porosity: 77.5% • Mean pore radius: 57.9 nm	[11]
Polydopamine coated ZnFe$_2$O$_4$	HA	4 wt%	• Pure water permeability: 687 L/m^2 h bar • HA removal: 82% • Porosity: 80% • Mean pore radius: 69 nm	[62]
PHEMA-grafted SiO$_2$	BSA	10 wt%	• Pure water permeability: 190 L/m^2 h bar • BSA removal: 75.5%	[63]

3. Materials and Methods

3.1. Reagents and Standarts

FeCl$_3$·6H$_2$O, FeCl$_2$·4H$_2$O, citric acid, PDX (polydioxanone), Leu-Gly (leucyl-glycine), 1,1,1,3,3,3-Hexafluoro-2-propanol (HFIP), *N*-Hydroxysuccinimide (NHS), *N*-(3-Dimethylaminopropyl)-*N'*-ethylcarbodiimide hydrochloride (EDC), bovine serum albumin (BSA (MW: 66,000 g/mol)), and dimethyl sulfoxide (DMSO) were supplied from Sigma-Aldrich (Darmstad, Germany), while a PES with a 58,000 g/mol molecular weight was supplied from BASF. Ultrapure water and analytical reagent-grade chemicals were used in the experiments.

3.2. Instrumentation

The Fe concentrations in the nanoparticles were measured by a method in our recent study [64]. The infrared spectra of the nanoparticles were recorded on a FT-IR (Perkin Elmer, Waltham, MA, USA). The magnetic properties of the materials were investigated by using a Model P525 Vibrating Sample Magnetometer (VSM) measurement system (Quantum Design, San Diego, CA, USA) at 27 °C. A LEO-Evo 40 XVP SEM was used to monitor the surface macrostructure (200 kV, 0.5 nm probe size).

3.3. Synthesis Procedure

The γ-Fe$_2$O$_3$-CA-Leu-Gly was further coated with PDX, a biodegradable poly(ester-ether). Many surgical sutures, as well as unperforated plates, straight pins, and medical clips are made of PDX [65]. In addition, PDX can be used as the biomaterial for biotechnological applications [66]. According to our literature survey, this study is the first to use PDX as a coating material. The γ-Fe$_2$O$_3$ magnetic nanoparticles were synthesized by a well-known chemical precipitation method. NH$_4$OH was used as the basic reagent. FeCl$_3 \cdot$6H$_2$O and FeCl$_2 \cdot$4H$_2$O (with a mole ratio of 2:1) were dissolved in water and ultra-sonicated for 10 min. A 10 mL amount of 5% NH$_4$OH was added with a 0.1 mL/min flow rate at 70 °C [64,67]. An amount of 100 mg of citric acid (CA) was added to the mixture and stirred at 80 °C for 30 min [68]. This was dried in a vacuum oven after washing to neutral by water. The carboxylated magnetic nanoparticle (γ-Fe$_2$O$_3$-CA) was then added with 0.08 g of NHS and 100 µL of EDC dissolved in PBS [69]. After an addition of Leu-Gly in PBS, it was mixed at 10 °C overnight. The functionalized magnetic nanoparticles were separated by a NdFeB magnet. This was added with a 0.1% solution of PDX in water: HFIP (1:1 *v/v*) and refluxed at 10 °C overnight. The final product was separated by the NdFeB magnet and dried in a vacuum oven.

3.4. Characterization of γ-Fe$_2$O$_3$-CA-Leu-Gly-PDX

Approximately 0.01 g of magnetic nanoparticle was weighted and digested with HCl: HNO$_3$:H$_2$O$_2$ (3:1:0.5 *v/v/v*). After drying on a heater, the residues were dissolved in 1.0 mol/L HNO$_3$. The concentrations of Fe were measured by ICP-OES. The FT-IR spectra were comparatively evaluated to investigate the surface functionality. XRD was used to determine the chemical structure of the composite PES membrane. VSM was employed to determine the magnetic saturation value at 25 °C. The surface macrostructure was investigated by a SEM.

3.5. Biological Activity of γ-Fe$_2$O$_3$-CA-Leu-Gly-PDX Nanoparticles

3.5.1. DPPH Activity

The radical scavenging activity of the γ-Fe$_2$O$_3$-CA-Leu-Gly-PDX by the 2,2-diphenyl-1-picrylhydrazyl (DPPH) method was investigated with some modifications [70]. A 250 µL amount of γ-Fe$_2$O$_3$-CA-Leu-Gly-PDX at 12.5–200 mg/L concentrations was incubated with 1000 µL of DPPH solution in methanol for 30 min in dark conditions. Afterwards, the radical scavenging ability was measured by a spectrophotometer at 517 nm. Trolox and ascorbic acid were used as the standard antioxidants.

3.5.2. Ferrous Ion Chelating Activity

The metal chelating ability of the γ-Fe$_2$O$_3$-CA-Leu-Gly-PDX was tested by the Dinis method [71]. The test γ-Fe$_2$O$_3$-CA-Leu-Gly-PDX at different concentrations was added with FeCI$_2$ and ferrozine. The metal chelating activity was measured after 10 min of waiting in dark conditions at 562 nm.

3.5.3. Antimicrobial Activity

The antimicrobial activity of the γ-Fe$_2$O$_3$-CA-Leu-Gly-PDX was examined using a broth microdilution assay. *Candida tropicalis* (ATCC 750), *Pseudomonas aeruginosa* (ATCC 27853), *Enterococcus faecalis* (ATCC 29212), *Escherichia coli* (ATCC 25922), *Staphylococcus aureus* (ATCC 25923), *Enterococcus hirae* (ATCC 10541), *Candida parapisilosis* (ATCC 22019) and *Legionella pneumophila subsp. pneumophila* (ATCC 33152) were used as the microbial strains.

They were firstly grown before the dilution step to obtain a fresh culture. Two-fold serial dilutions of the γ-Fe$_2$O$_3$-CA-Leu-Gly-PDX were performed, and the test microorganisms were inoculated to the microplate-wells before incubation in an oven (for 24 h, at 37 °C). When the incubation was finished, the minimum inhibition concentration (MIC) values were determined.

3.5.4. DNA Cleavage Ability

Plasmid pBR322 DNA was used to investigate the DNA cleavage ability of the γ-Fe$_2$O$_3$-CA-Leu-Gly-PDX. Plasmid DNA at 0.1 mg/L was added with different concentrations of γ-Fe$_2$O$_3$-CA-Leu-Gly-PDX (for 90 min, at 37 °C) before agarose gel electrophoresis to measure the activity of the γ-Fe$_2$O$_3$-CA-Leu-Gly-PDX. A transilluminator was used for visualization of the DNA molecules.

3.5.5. Bacterial Viability Test

E. coli (ATCC 10536) was used to investigate the microbial cell viability. A nutrient broth was used for the inoculation of the *E. coli* culture by incubating at 37 °C (for 24 h, at 150 rpm). Then, it was centrifuged (at 5000 rpm, for 5 min). The culture media residuals were removed by washing with a 0.85% sterile saline solution and suspended in a NaCl solution (10 mL). Then, different concentrations of γ-Fe$_2$O$_3$-CA-Leu-Gly-PDX were added and incubated (at 37 °C, for 90 min).

They were then diluted in various rates, inoculated in solid media and left to incubate at 37 °C for 24 h. A control group without γ-Fe$_2$O$_3$-CA-Leu-Gly-PDX was employed with the same procedure.

3.5.6. Antimicrobial Photodynamic Therapy by γ-Fe$_2$O$_3$-CA-Leu-Gly-PD

E. coli was incubated with γ-Fe$_2$O$_3$-CA-Leu-Gly-PD at concentrations of 25 and 50 mg/L in the dark (15 min, 37 °C) and then an LED light irradiation was applied for 10 min. After exposure to the LED light, they were then diluted at different rates. After dilution, they were inoculated in solid NB media and further incubated (for 24 h, at 37 °C). The control group without γ-Fe$_2$O$_3$-CA-Leu-Gly-PDX was employed with same procedure. Then, the colonies were counted and the antimicrobial photodynamic therapy by the γ-Fe$_2$O$_3$-CA-Leu-Gly-PD was calculated.

3.5.7. Biofilm Inhibition Activity

The possible effect of synthesized γ-Fe$_2$O$_3$-CA-Leu-Gly-PD on the biofilm inhibition of *P. aeruginosa* and *S. aureus* was investigated. Test microorganisms were incubated with 125, 250 and 500 mg/L concentrations of γ-Fe$_2$O$_3$-CA-Leu-Gly-PD at 37 °C for 72 h. Then, the plates were emptied, washed and dried (at 80 °C, for 20 min). After 30 min, there was an addition of crystal violet (CV). The plates were washed twice to remove excessive CV, then adsorbed CV on the plates was recovered by adding ethanol and waiting for 15 min. The concentration of CV in the recovered solution was measured by using a spectrophotometer (595 nm). The control group without γ-Fe$_2$O$_3$-CA-Leu-Gly-PDX was employed with the same procedure. The biofilm inhibition was used for the calculations.

3.6. Membrane Experiments

3.6.1. Preparation of γ-Fe$_2$O$_3$-CA-Leu-Gly-PDX-Blended PES Membrane

A phase inversion method was used to prepare the pristine and γ-Fe$_2$O$_3$-CA-Leu-Gly-PDX NPs-blended PES membranes. DMSO was used to solve the polymer [72]. Briefly, 1.0 wt% of nanoparticles (NPs) and 85 wt% of DMSO were mixed and ultra-sonicated to provide a complete dispersion of NPs into the DMSO. After the addition of PES (14%), this was shaken at room temperature overnight. The membrane was cast with a 200 μm thickness at a speed of 100 mm/s.

The mean pore size (nm) was determined from the flux and porosity results via the Elford–Ferry equation [73]. A gravimetric analysis was performed to determine the porosity of the prepared membranes [74].

3.6.2. Protein Rejection Experiments of the Membranes

Performance characteristics of the membranes were tested by using a dead-end filtration system (with a 300 mL cell capacity, and 14.6 cm^2 as the effective area). A 5-bar operation pressure (30 min) was applied to the membrane for compaction. Then, the

pressure was reduced to a 3-bar level and a pure water flux was measured (for 15 min). A 50 mg/L amount of the BSA solution was used as the model organic foulant and used to fill the cells. The permeation of BSA was measured at the 3-bar level (for 60 min). Afterwards, the fouled membranes were washed with deionized water. Lastly, the pure water flux after rinsing was measured for 15 min at a steady pressure of the 3-bar level.

The Lowry method was used to determine the protein concentration of the feed and the permeate at 660 nm using a spectrophotometer (GBC-Cintra-20) [75].

3.6.3. Application of γ-Fe$_2$O$_3$-CA-Leu-Gly-PDX-Blended PES Membrane for *E. coli* Removal

The *E. coli* (ATCC 25922) was cultured in a 100 mL glass bottle including 25 mL of NB (at 120 rpm and 37 °C, for 24 h). Then, the culture was diluted with a 0.9% sterile NaCl solution and was filtrated through the membranes, where the permeate was collected after 120 min of filtration. After dilution, the inlet and permeate *E. coli* solution was incubated at 37 °C for 24 h on the NB solid media. Finally, the growth inhibition (%) was calculated considering the colony count.

4. Conclusions

Hereby, we present the synthesis and characterization of a γ-Fe$_2$O$_3$-CA-Leu-Gly-PDX-modified PES membrane for biotechnological applications. The DPPH activity, radical scavenging activity, and metal chelating activity were investigated as well as the antimicrobial, DNA cleavage, microbial cell viability, and antimicrobial photodynamic therapy properties. The nanocomposite membranes demonstrated remarkable antifouling properties in contrast with the pristine PES when BSA and *E. coli* were filtrated. The modified polyethersulphone (PES) membrane blended with the γ-Fe$_2$O$_3$-CA-Leu-Gly-PDX removed 100% of the *E. Coli.* By considering the results achieved from this study, we can recommend the use of a γ-Fe$_2$O$_3$-CA-Leu-Gly-PDX-modified PES membrane for routine biotechnological applications. Additionally, it should be highlighted that the magnetic and biocompatible functionalization of PES will importantly contribute to the current science.

Author Contributions: Conceptualization, N.D. and E.K.; methodology, N.D.; software, S.Ö.; validation, N.D., E.K. and Ö.D.; formal analysis, Ö.D.; investigation, S.G.; resources, Ö.D. and S.G.; data curation, V.T.; writing—original draft preparation, N.D. and E.K.; writing—review and editing, V.T. and S.Ö.; visualization, S.G.; supervision, Ö.D.; project administration, N.D., E.K. and S.Ö.; funding acquisition, E.K. All authors have read and agreed to the published version of the manuscript.

Data Availability Statement: Not applicable.

Conflicts of Interest: The authors declare no conflict of interest.

References

1. Son, M.; Choi, H.; Liu, L.; Park, H.; Choie, H. Optimized synthesis conditions of polyethersulfone support layer for enhanced water flux for thin film composite membrane. *Environ. Eng. Res.* **2014**, *19*, 339–344. [CrossRef]
2. Mathaba, M.; Daramola, M.O. Effect of chitosan's degree of deacetylation on the performance of PES membrane infused with chitosan during AMD treatment. *Membranes* **2020**, *10*, 52. [CrossRef] [PubMed]
3. Patil, H.; Shanmugam, V.; Marathe, K. Studies in synthesis and modification of PES membrane and its application for removal of reactive black 5 dye. *Ind. Chem. Eng.* **2022**, *64*, 111–120. [CrossRef]
4. Altass, H.M.; Morad, M.; Khder, A.E.S.; Mannaa, M.A.; Jassas, R.S.; Alsimaree, A.A.; Ahmed, S.A.; Salama, R.S. Enhanced catalytic activity for CO oxidation by highly active Pd nanoparticles supported on reduced graphene oxide/copper metal organic framework. *J. Taiwan Inst. Chem. Eng.* **2021**, *128*, 194–208. [CrossRef]
5. Krishnamoorthy, R.; Sagadevan, V. Polyethylene glycol and iron oxide nanoparticles blended polyethersulfone ultrafiltration membrane for enhanced performance in dye removal studies. *E-polymers* **2015**, *15*, 151–159. [CrossRef]
6. Yu, M.; Renner, J.N.; Duval, C.E. A lysine-modified polyethersulfone (PES) membrane for the recovery of lanthanides. *Front. Chem.* **2020**, *8*, 512–522. [CrossRef]

7. Ghaemi, N.; Madaeni, S.S.; Daraei, P.; Rajabi, H.; Zinadini, S.; Alizadeh, A.; Heydari, R.; Beygzadeh, M.; Ghouzivand, S. Polyethersulfone membrane enhanced with iron oxide nanoparticles for copper removal from water: Application of new functionalized Fe_3O_4 nanoparticles. *Chem. Eng. J.* **2015**, *263*, 101–112. [CrossRef]

8. Kouhestani, F.; Torangi, M.A.; Motavalizadehkakhky, A.; Karazhyan, R.; Zhiani, R. Enhancement strategy of polyethersulfone (PES) membrane by introducing pluronic F127/graphene oxide and phytic acid/graphene oxide blended additives: Preparation, characterization and wastewater filtration assessment. *Desalin. Water Treat.* **2019**, *171*, 44–56. [CrossRef]

9. Qadir, D.; Mukhtar, H.; Keong, L.K. Synthesis and characterization of polyethersulfone/carbon molecular sieve based mixed matrix membranes for water treatment applications. *Procedia Eng.* **2016**, *148*, 588–593. [CrossRef]

10. Marjani, A.; Nakhjiri, A.T.; Adimi, M.; Jirandehi, H.F.; Shirazian, S. Effect of graphene oxide on modifying polyethersulfone membrane performance and its application in wastewater treatment. *Sci. Rep.* **2020**, *10*, 2049–2059. [CrossRef]

11. Ouda, M.; Hai, A.; Krishnamoorthy, R.; Govindan, B.; Othman, I.; Kui, C.C.; Choi, M.Y.; Hasan, S.W.; Banat, F. Surface tuned polyethersulfone membrane using an iron oxide functionalized halloysite nanocomposite for enhanced humic acid removal. *Environ. Res.* **2022**, *204*, 112113. [CrossRef]

12. Abidin, M.N.Z.; Goh, P.S.; Ismail, A.F.; Said, N.; Othman, M.H.D.; Hasbullah, H.; Abdullah, M.S.; Ng, B.C.; Kadir, S.H.S.A.; Kamal, F. Polysulfone/iron oxide nanoparticles ultrafiltration membrane for adsorptive removal of phosphate from aqueous solution. *J. Membr. Sci. Res.* **2019**, *5*, 20–24.

13. Machodi, M.J.; Daramola, M.O. Synthesis of PES and PES/chitosan membranes for synthetic acid mine drainage treatment. *Water SA* **2020**, *46*, 114–122.

14. Wen, Y.; Yuan, J.; Ma, X.; Wang, S.; Liu, Y. Polymeric nanocomposite membranes for water treatment: A review. *Environ. Chem. Let.* **2019**, *17*, 1539–1551. [CrossRef]

15. Alshorifi, F.T.; Alswat, A.A.; Salama, R.S. Gold-selenide quantum dots supported onto cesium ferrite nanocomposites for the efficient degradation of rhodamine B. *Heliyon* **2022**, *8*, e09652. [CrossRef]

16. Zhao, C.X.; Ran, J.; Sun, F.S. Modification of polyethersulfone membranes—A review of methods. *Prog. Mater. Sci.* **2013**, *58*, 76–150. [CrossRef]

17. Ocakoglu, K.; Dizge, N.; Colak, S.G.; Ozay, Y.; Bilici, Z.; Yalcin, M.S.; Ozdemir, S.; Yatmaz, H.C. Polyethersulfone membranes modified with CZTS nanoparticles for protein and dye separation: Improvement of antifouling and self-cleaning performance. *Colloids Surf. A Physicochem. Eng.* **2021**, *616*, 126230. [CrossRef]

18. Abdulkarem, E.; Ibrahim, Y.; Naddeo, V.; Banat, F.; Hasan, S.W. Development of Polyethersulfone/α-Zirconium phosphate (PES/α-ZrP) flat-sheet nanocomposite ultrafiltration membranes. *Chem. Eng. Res. Des.* **2020**, *161*, 206–217. [CrossRef]

19. Vatanpour, V.; Khadem, S.S.M.; Dehqan, A.; Naqshabandi, M.A.; Ganjali, M.R.; Hassani, S.S.; Rashid, M.R.; Saeb, M.R.; Dizge, N. Efficient removal of dyes and proteins by nitrogen-doped porous graphene blended polyethersulfone nanocomposite membranes. *Chemosphere* **2021**, *263*, 127892. [CrossRef]

20. Vatanpour, V.; Paziresh, S.; Dehqan, A.; Asadzadeh-Khaneghah, S.; Habibi-Yangjeh, A. Hydrogen peroxide treated g-C_3N_4 as an effective hydrophilic nanosheet for modification of polyethersulfone membranes with enhanced permeability and antifouling characteristics. *Chemosphere* **2021**, *279*, 130616. [CrossRef]

21. Yogarathinam, L.T.; Goh, P.S.; Ismail, A.F.; Gangasalam, A.; Ahmad, N.A.; Samavati, A.; Mamah, S.C.; Abidin, M.N.Z.; Ng, B.C.; Gopal, B. Nanocrystalline cellulose incorporated biopolymer tailored polyethersulfone mixed matrix membranes for efficient treatment of produced water. *Chemosphere* **2022**, *293*, 133561. [CrossRef]

22. Abbas, T.T.; Rashid, T.K.; Alsalhy, Q.F. NaY zeolite-polyethersulfone-modified membranes for the removal of cesium-137 from liquid radioactive waste. *Chem. Eng. Res. Des.* **2022**, *179*, 535–548. [CrossRef]

23. Qi, G.B.; Gao, Y.J.; Wang, L.; Wang, H. Self-assembled peptide-based nanomaterials for biomedical imaging and therapy. *Adv. Mater.* **2018**, *30*, 1703444. [CrossRef]

24. Park, J.; Lee, J.E.; Shin, H.J.; Song, S.; Hwang, J.S. Oral administration of glycine and leucine dipeptides improves skin hydration and elasticity in UVB-irradiated hairless mice. *Biomol. Ther.* **2017**, *25*, 528–534. [CrossRef]

25. Vanhoye, D.; Bruston, F.; Amri, S.E.; Ladram, A.; Amiche, M.; Nicolas, P. Membrane association, electrostatic sequestration, and cytotoxicity of Gly-Leu-rich peptide orthologs with differing functions. *Biochemistry* **2004**, *43*, 8391–8409. [CrossRef]

26. Fields, G.B. Synthesis and biological applications of collagen-model triplehelical peptides. *Org. Biomol. Chem.* **2010**, *8*, 1237–1258. [CrossRef]

27. Roushenasa, P.; Yusop, Z.; Majidnia, Z.; Nasdrollahpour, R. Photocatalytic degradation of spilled oil in sea water using maghemite nanoparticles. *Desalin. Water Treat.* **2016**, *57*, 5837–5841. [CrossRef]

28. Goonoo, N.; Bhaw-Luximon, A.; Jonas, U.; Jhurry, D.; Schönherr, H. Enhanced differentiation of human preosteoblasts on electrospun blend fiber mats of polydioxanone and anionic sulfated polysaccharides. *ACS Biomater. Sci. Eng.* **2017**, *3*, 3447–3458. [CrossRef]

29. Bartolome, L.; Imran, M.; Lee, K.G.; Sanglang, A.; Ahn, J.K.; Kim, D.Y. Superparamagnetic γ-Fe_2O_3 is applied as efficient, easily recoverable, and reusable catalyst for the chemical recycling of PET via glycolysis. *Green Chem.* **2014**, *16*, 279–286. [CrossRef]

30. Kılınç, E. Fullerene C60 functionalized γ-Fe_2O_3 magnetic nanoparticle: Synthesis, characterization and biomedical application. *Artif. Cells Nanomed. Biotechnol.* **2016**, *44*, 298–304. [CrossRef]

31. Guivar, J.A.R.; Sanches, E.A.; Bruns, F.; Sadrollahi, E.; Morales, M.A.; Lopez, E.O.; Litterst, F.J. Vacancy ordered-Fe$_2$O$_3$ nanoparticles functionalized with nanohydroxyapatite: XRD, FTIR, TEM, XPS and Mössbauer studies. *Appl. Surf. Sci.* **2016**, *389*, 721–734. [CrossRef]

32. Yang, K.K.; Wang, X.L.; Wang, Y.Z. Poly(*p*-dioxanone) and its copolymers. *J. Macromol. Sci. E Part C—Polym. Rev.* **2002**, *C42*, 373–398. [CrossRef]

33. Abdullah, J.A.A.; Eddine, L.S.; Abderrhmane, B.; Alonso-Gonzalez, M.; Romero, G.A. Green synthesis and characterization of iron oxide nanoparticles by *Phoenix dactylifera* leaf extract and evaluation of their antioxidant activity. *Sustain. Chem. Pharm.* **2020**, *17*, 100280. [CrossRef]

34. Erci, F.; Cakir-Koc, R. Rapid green synthesis of noncytotoxic iron oxide nanoparticles using aqueous leaf extract of *Thymbra spicata* and evaluation of their antibacterial, antibiofilm, and antioxidant activity. *Inorg. Nano-Metal. Chem.* **2021**, *51*, 683–692. [CrossRef]

35. Yeğenoğlu, H.; Aslım, B.; Güven, B.; Zengin, A.; Boyacı, İ.H.; Suludere, Z.; Tamer, İ. The comparison of antioxidant capacity and cytotoxic, anticarcinogenic, and genotoxic effects of Fe@Au nanosphere magnetic nanoparticles. *Turk. J. Biol.* **2017**, *41*, 302–313. [CrossRef]

36. Shah, S.T.; Yehya, W.A.; Saad, O.; Simarani, K.; Chowdhury, Z.; Alhadi, A.A.; Al-Ani, L.A. Surface functionalization of iron oxide nanoparticles with gallic acid as potential antioxidant and antimicrobial agents. *Nanomaterials* **2017**, *7*, 306. [CrossRef]

37. Madhu, G.C.; Jaianand, K.; Rameshkumar, K.; Eyini, M.; Balaji, P.; Veeramanikandan, V. *Solanum tuberosum* extract mediated synthesis and characterization of iron oxide nanoparticles for their antibacterial and antioxidant activity. *J. Drug Deliv. Ther.* **2019**, *9*, 15. [CrossRef]

38. Rufus, N.S.; Philip, D. Synthesis of biogenic hematite (α-Fe$_2$O$_3$) nanoparticles for antibacterial and nanofluid applications. *RSC Adv.* **2016**, *6*, 94206–94217. [CrossRef]

39. Naseem, T.; Farrukh, M.A. Antibacterial activity of green synthesis of iron nanoparticles using *Lawsonia inermis* and *Gardenia jasminoides* leaves extrac. *J. Chem.* **2015**, *2015*, 912342. [CrossRef]

40. Rafi, M.M.; Ahmed, K.S.Z.; Nazeer, K.P.; Kumar, D.S.; Thamilselvan, M. Synthesis, characterization and magnetic properties of hematite (α-Fe$_2$O$_3$) nanoparticles on polysaccharide templates and their antibacterial activity. *Appl. Nanosci.* **2015**, *5*, 515–520. [CrossRef]

41. Khalid, H.F.; Tehseen, B.; Sarwar, Y.; Hussain, S.Z.; Khan, W.S.; Raza, Z.A.; Bajwa, S.Z.; Kanaras, A.G.; Hussain, I.; Rehman, A. Biosurfactant coated silver and iron oxide nanoparticles with enhanced anti-biofilm and anti-adhesive properties. *J. Hazard. Mater.* **2019**, *364*, 441–448. [CrossRef]

42. Moos, N.; Slaveykova, V.I. Oxidative stress induced by inorganic nanoparticles in bacteria and aquatic microalgae–state of the art and knowledge gaps. *Nanotoxicology* **2014**, *8*, 605–630. [CrossRef]

43. Turakhia, B.; Chikkala, S.; Shah, S. Novelty of bioengineered iron nanoparticles in nano coated surgical cotton: A green chemistry. *Adv. Pharmacol. Sci.* **2019**, *2019*, 9825969.

44. Shi, S.F.; Jia, J.F.; Guo, X.K.; Zhao, Y.P.; Chen, D.S.; Guo, Y.Y.; Zhang, X.L. Reduced *Staphylococcus aureus* biofilm formation in the presence of chitosan-coated iron oxide nanoparticles. *Int. J. Nanomed.* **2016**, *11*, 6499–6506. [CrossRef]

45. Inbaraj, B.S.; Kao, T.H.; Tsai, T.Y.; Chiu, C.P.; Kumar, R.; Chen, B.H. The synthesis and characterization of poly(gamma-glutamic acid)-coated magnetite nanoparticles and their effects on antibacterial activity and cytotoxicity. *Nanotechnology* **2011**, *22*, 075101. [CrossRef]

46. Chen, X.; Hu, B.; Xiang, Q.; Yong, C.; Liu, Z.; Xing, X. Magnetic nanoparticles modified with quaternarized *N*-halamine based polymer and their antibacterial properties. *J. Biomater. Sci. Polym. Ed.* **2016**, *27*, 1187–1199. [CrossRef]

47. Niemirowicz, K.; Surel, U.; Wilczewska, A.Z.; Mystkowska, J.; Piktel, E.; Gu, X.; Namiot, Z.; Kułakowska, A.; Savage, P.B.; Bucki, R. Bactericidal activity and biocompatibility of ceragenin-coated magnetic nanoparticles. *J. Nanobiotechnol.* **2015**, *13*, 32. [CrossRef]

48. Pu, L.; Xu, J.; Sun, Y.; Fang, Z.; Chan-Park, M.B.; Duan, H. Cationic polycarbonate-grafted superparamagnetic nanoparticles with synergistic dual-modality antimicrobial activity. *Biomater. Sci.* **2016**, *4*, 871–879. [CrossRef]

49. Venkatesan, K.; Babu, D.R.; Bai, M.P.K.; Supriya, R.; Vidya, R.; Madeswaran, S.; Anandan, P.; Arivanandhan, M.; Hayakawa, Y. Structural and magnetic properties of cobaltdoped iron oxide nanoparticles prepared by solution combustion method for biomedical applications. *Int. J. Nanomed.* **2015**, *10*, 189–198.

50. Zomorodian, K.; Veisi, H.; Mousavi, S.M.; Ataabadi, M.S.; Yazdanpanah, S.; Bagheri, J.; Mehr, A.P.; Hemmati, S.; Veisi, H. Modified magnetic nanoparticles by PEG-400-immobilized Ag nanoparticles (Fe$_3$O$_4$@PEG-Ag) as a core/shell nanocomposite and evaluation of its antimicrobial activity. *Int. J. Nanomed.* **2018**, *13*, 3965–3973. [CrossRef]

51. Rehana, D.; Haleel, A.K.; Rahiman, A.K. Hydroxy, carboxylic and amino acid functionalized superparamagnetic iron oxide nanoparticles: Synthesis, characterization and in vitro anti-cancer studies. *J. Chem. Sci.* **2015**, *127*, 1155–1166. [CrossRef]

52. Palchoudhury, S.; Xu, Y.; Rushdi, A.; Bao, Y. DNA interaction of Pt-attached iron oxide nanoparticles. *IEEE Trans. Magn.* **2013**, *9*, 373–376. [CrossRef]

53. Antonoglou, O.; Lafazanis, K.; Mourdikoudis, S.; Vourlias, G.; Lialiaris, T.; Pantazaki, A.; Dendrinou-Samara, C. Biological relevance of CuFeO$_2$ nanoparticles: Antibacterial and anti-inflammatory activity, genotoxicity, DNA and protein interactions. *Mater. Sci. Eng. C* **2019**, *99*, 264–274. [CrossRef]

54. Gold, K.; Slay, B.; Knackstedt, M.; Gaharwar, A.K. Antimicrobial activity of metal and metal-oxide based nanoparticles. *Adv. Therap.* **2018**, *1*, 1700033. [CrossRef]

55. Naha, P.C.; Liu, Y.; Hwang, G.; Huang, Y.; Gubara, S.; Jonnakuti, V.; Simon-Soro, A.; Kim, D.; Gao, L.; Koo, H.; et al. Dextran-coated iron oxide nanoparticles as biomimetic catalysts for localized and pH-activated biofilm disruption. *ACS Nano.* **2019**, *13*, 4960–4971. [CrossRef]

56. Sathyanarayanan, M.B.; Balachandranath, R.; Srinivasulu, Y.G.; Kannaiyan, S.K.; Subbiahdoss, G. The effect of gold and iron-oxide nanoparticles on biofilm-forming pathogens. *ISRN Microbiol.* **2013**, *2013*, 272086. [CrossRef]

57. Carrera, E.T.; Dias, H.B.; Corbi, S.C.T.; Marcantonio, R.A.C.; Bernardi, A.C.A.; Bagnato, V.S.; Hamblin, M.R.; Rastelli, A.N.S. The application of antimicrobial photodynamic therapy (aPDT) in dentistry: A critical review. *Laser Phys.* **2016**, *26*, 123001. [CrossRef]

58. Ma, S.; Zhan, S.; Jia, Y.; Zhou, Q. Superior antibacterial activity of Fe_3O_4-TiO_2 nanosheets under solar light. *ACS Appl. Mater. Interfaces* **2015**, *7*, 21875–21883. [CrossRef]

59. Pan, W.Y.; Huang, C.C.; Lin, T.T.; Hu, H.Y.; Lin, W.C.; Li, M.J.; Sung, H. Synergistic antibacterial effects of localized heat and oxidative stress caused by hydroxyl radicals mediated by graphene/iron oxide-based nanocomposites. *Nanomedicine* **2016**, *12*, 431–438. [CrossRef]

60. Thukkaram, M.; Sitaram, S.; Kannaiyan, S.K.; Subbiahdoss, G. Antibacterial efficacy of iron-oxide nanoparticles against biofilms on different biomaterial surfaces. *Int. J. Biomat.* **2014**, *2014*, 716080. [CrossRef]

61. Armijo, L.M.; Wawrzyniec, S.J.; Kopicuch, M.; Brandt, Y.I.; Rivera, A.C.; Withers, N.J.; Cook, N.C.; Huber, D.L.; Monson, T.C.; Smyth, H.D.C.; et al. Antibacterial activity of iron oxide, ron nitride, and tobramycin conjugated nanoparticles against Pesudoonas aeruginosa biofilms. *J. Nanobiotechnol.* **2020**, *18*, 35. [CrossRef] [PubMed]

62. Kallem, P.; Othman, I.; Ouda, M.; Hasan, S.W.; AlNashef, I.; Banat, F. Polyethersulfone hybrid ultrafiltration membranes fabricated with polydopamine modified $ZnFe_2O_4$ nanocomposites: Applications in humic acid removal and oil/water emulsion separation. *Process Saf. Environ. Prot.* **2021**, *148*, 813–824. [CrossRef]

63. Zhu, L.J.; Zhu, L.P.; Jiang, J.H.; Yi, Z.; Zhao, Y.F.; Zhu, B.K.; Xu, Y.Y. Hydrophilic and anti-fouling polyethersulfone ultrafiltration membranes with poly (2-hydroxyethyl methacrylate) grafted silica nanoparticles as additive. *J. Memb. Sci.* **2014**, *451*, 157–168. [CrossRef]

64. Kılınç, E. γ-Fe_2O_3 magnetic nanoparticle functionalized with carboxylated multi walled carbon nanotube: Synthesis, characterization, analytical and biomedical applications. *J. Magn. Magn. Mater.* **2016**, *401*, 949–955. [CrossRef]

65. Martins, J.A.; Lach, A.A.; Morris, H.L.; Carr, A.J.; Mouthuy, P.A. Polydioxanone implants: A systematic review on safety and performance in patients. *J. Biomater. Appl.* **2020**, *34*, 902–916. [CrossRef]

66. Goonoo, N.; Jeetah, R.; Bhaw-Luximon, A.; Jhurry, D. Polydioxanone-based bio-materials for tissue engineering and drug/gene delivery applications. *Eur. J. Pharm. Biopharm.* **2015**, *97*, 371–391. [CrossRef]

67. Darezereshki, E. Synthesis of maghemite (γ-Fe_2O_3) nanoparticles by wet chemical method at room temperature. *Mater. Lett.* **2010**, *64*, 1471–1472. [CrossRef]

68. Sousa, M.E.; Raap, M.B.F.; Rivas, P.C.; Zelis, P.M.; Girardin, P.; Pasquevich, G.A.; Alessandrini, J.L.; Muraca, D.; Sanchez, F.E. Stability and relaxation mechanisms of citric acid coated magnetite nanoparticles for magnetic hyperthermia. *J. Phys. Chem. C* **2013**, *117*, 5436–5445. [CrossRef]

69. Yiu, H.H.P.; Keane, M.A. Enzyme–magnetic nanoparticle hybrids: New effective catalysts for the production of high value chemicals. *Chem. Technol. Biotechnol.* **2012**, *87*, 583–594. [CrossRef]

70. Agırtaş, M.S.; Karatas, C.; Özdemir, S. Synthesis of some metallophthalocyanines with dimethyl 5-(phenoxy)-isophthalate substituents and evaluation of their antioxidant-antibacterial activities, Spectrochim. *Acta A Mol. Biomol. Spectros.* **2015**, *135*, 20–24. [CrossRef]

71. Dinis, T.C.P.; Madeira, V.M.C.; Almeida, L.M. Action of phenolic derivatives (acetaminophen, salicylate, and 5-aminosalicylate) as inhibitors of membrane lipid peroxidation and as peroxyl radical scavengers. *Arch. Biochem. Biophys.* **1994**, *315*, 161–169. [CrossRef]

72. Bilici, Z.; Ozay, Y.; Yuzer, A.; Ince, M.; Ocakoglu, K.; Dizge, N. Fabrication and characterization of polyethersulfone membranes functionalized with zinc phthalocyanines embedding different substitute groups. *Colloids Surf. A Physicochem. Eng.* **2021**, *617*, 126288. [CrossRef]

73. Gumbi, N.N.; Hu, M.; Mamba, B.B.; Li, J.; Nxumalo, E.N. Macrovoid-free PES/SPSf/O-MWCNT ultrafiltration membranes with improved mechanical strength, antifouling and antibacterial properties. *J. Memb. Sci.* **2018**, *566*, 288–300. [CrossRef]

74. Rambabu, K.; Gokul, S.; Russel, A.S.; Sivaramakrishna, A.; Ponnusami, B.; Banat, F. Lithium perchlorate modified nanoporous polyethersulfone membrane for improved dye rejection. *Desalin. Water Treat.* **2018**, *122*, 146–157. [CrossRef]

75. Lowry, O.H.; Rosebrough, N.; Farr, A.L.; Randall, R.J. Protein measurement with the folin phenol reagent. *J. Biol. Chem.* **1951**, *193*, 265–275. [CrossRef]